Evidence for cubic phase in deposited germanium nanocrystals

2003 J. Phys.: Condens. Matter 15 1017

(http://iopscience.iop.org/0953-8984/15/7/301)

INSTITUTE OF PHYSICS PUBLISHING JOURNAL OF PHYSICS: CONDENSED MATTER

J. Phys.: Condens. Matter **15** (2003) 1017–1028 PII: S0953-8984(03)57129-6

Evidence for cubic phase in deposited germanium nanocrystals

C Bostedt[1,2], T van Buuren[1], J M Plitzko[1,4], T Möller[3] and L J Terminello[1]

[1] Lawrence Livermore National Laboratory, PO Box 808, Livermore, CA 94550, USA
[2] Universität Hamburg, Institut für Experimentalphysik, Hamburg, Germany
[3] Hamburger Synchrotronstrahlungslabor Hasylab at DESY, Hamburg, Germany

Received 4 December 2002
Published 10 February 2003
Online at stacks.iop.org/JPhysCM/15/1017

Abstract

Germanium nanocrystals with sizes ranging from 1 to 5 nm are condensed out of the gas phase in helium or argon buffer-gas atmospheres and subsequently deposited. The generated particle sizes are found to depend on the buffer gas, with helium yielding a narrower size distribution than argon and argon exhibiting a stronger pressure dependence of the produced particle sizes. Structural analysis of nanoparticles with average sizes around 5 nm reveals the bulklike cubic (diamond) phase—in contrast to recent experiments which suggest the tetragonal phase for similar-sized particles. These results are explained in terms of particle formation dynamics.

1. Introduction

Nanometre-sized structures have attracted tremendous interest over the last decade due to their broad spectrum of size-dependent properties [1]. Germanium nanocrystals have drawn significant interest since the first reports about their blue luminescence [2]. Many studies have focused on the Ge-nanocrystal synthesis and a variety of production techniques have been suggested. These techniques include supersonic expansion [3], ion implantation [4], laser ablation [5], magnetron cosputtering [6], chemical vapour deposition [7], sol–gel processes [8] and solution chemistry [9, 10].

However, most of these techniques allow only limited size control of the produced germanium particles [3–9], or are extensive in their set-up [10]. Additionally, most preparation routes leave the particles with a non-exchangeable surface chemistry such as a SiO_2 host matrix [4–6, 8] or a chemical surfactant [9, 10] which is an undesirable property for precise electronic structure investigations [11, 12]. For this class of experiments a gas-phase based synthesis method, such as supersonic expansion [3], chemical vapour deposition [7] or the one described in this report, is preferable.

[4] Present address: Max Planck Institute for Biochemistry, Martinsried, Germany.

0953-8984/03/071017+12$30.00

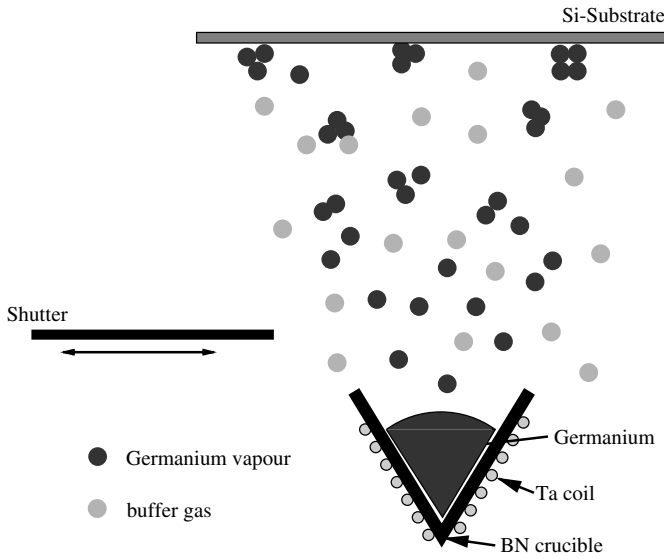

Figure 1. Basic principle of a gas-aggregation source: the cluster material is evaporated into an inert buffer-gas atmosphere. The vapour is cooled by ballistic collisions with the buffer gas, becomes supersaturated and small particles condense out. In the present experiment the clusters are subsequently deposited on a substrate. The mass flow is controlled with a mechanical shutter.

Experimentally, germanium nanocrystals produced with the supersonic-beam expansion have been found to exhibit the tetragonal phase [3]. Particles produced by means of chemical-vapour deposition have been found in the tetragonal, cubic and amorphous phases—depending on the synthesis parameters [7]. Theoretically, the cubic (diamond) phase has been predicted as the most stable phase for Ge nanoparticles [13].

In this paper we report on a gas-phase based synthesis method for supported germanium nanoparticles, which allows the production of ultra-clean nanocrystals with a narrow size distribution and a large tunable size range. First, the experimental setup is depicted. Second, the particle size distributions and the aggregation mechanisms are described. Third, the structural properties of the grown particles are investigated and discussed in light of other synthesis routes and recent theoretical studies.

2. Experimental details

A gas-aggregation nanocluster source has been developed for the synthesis of the germanium nanocrystals [14]. In figure 1 a schematic diagram of the nanoparticle source is shown. Germanium is evaporated into an inert buffer-gas atmosphere by resistive heating of a BN crucible in a tantalum filament. The produced germanium vapour is cooled by ballistic collisions with the buffer-gas atoms. It becomes supersaturated and small particles condense out. In the present experiment the clusters are subsequently deposited on a substrate $\sim$5 cm above the evaporator. The mass flow onto the substrate is controlled with a mechanical shutter, which sits in its 'closed' position only a few millimetres above the crucible to suppress the build-up of convection currents observed in earlier gas-aggregation experiments [15]. The evaporator temperatures are determined pyrometrically. Good reproducibility for the heating current–crucible temperature relationship has been observed. Therefore the heating current

has been utilized as experimental parameter within the experimental series as it is easier to determine and reference. Hereby the current necessary for melting the germanium (I_{melt} at $T_{melt} = 937\,^{\circ}\mathrm{C}$) has been found to be a reliable reference point for the absolute crucible temperature and thus cluster condensation process. For this reason a relative heating current I_{rel} is introduced, which is defined as $I_{rel} = I - I_{melt}$ as a convenient parameter for the discussion of the following cluster experiments.

The nanoparticle sizes and layer morphologies are probed with a molecular imaging Picoscan atomic force microscope (AFM) in magnetic AC (MAC) mode [16]. This mode exhibits very low tip–surface interaction [16] and thus is well suited for loosely bound nanoparticle samples. The AFM apparatus sits in a vibration isolation box to eliminate effects of building noise. The scanner used has a horizontal range of 6 μm and a vertical range of 2 μm. The lateral resolution of the AFM is determined by the tip radius due to the fact that the lateral AFM information is the convolution of the surface feature with the AFM tip. The vertical resolution depends only on the piezoelectric scanner and is according to manufacturer specifications in the Ångström regime. For these reasons the particle height over the baseline is measured as particle size and the particles are assumed to be spherical. To do so, a cross-sectional cut of the AFM micrograph is taken in the scan direction through the maximum height of the particle. The piezoelectric scanner has been calibrated with a standard and the calibration has been confirmed on step-edges of highly orientated pyrolytic graphite (HOPG) on a regular basis.

Transmission electron microscopy (TEM) experiments have been performed for investigation of the structural properties and confirmation of the AFM size measurements. The microscope used is a Philips TEM operated at 300 keV acceleration voltage, equipped with a field emission gun. The point-to-point resolution of this instrument is 2.2 Å. The particle structure is probed with high-resolution transmission electron microscopy (HRTEM) on the individual nanocrystal level as well as with selected area diffraction (SAD) in a sample-averaging mode. The particle size information is obtained in HRTEM.

3. Results and discussion

3.1. Nanoparticle generation

In figure 2 an AFM image of germanium nanoparticles on the basal plane of an HOPG surface is shown. The nanoclusters have been condensed in a helium atmosphere of 500 mTorr and a relative evaporation current of $I_{rel} = 3$ A ($\approx$1150 °C). The AFM image (figure 2) has x–y dimensions of 400 nm and a z scale of 2.7 nm. The nanoparticles shown exhibit a height around 2.1 nm. Their size distribution will be discussed in more detail below. It can be seen in figure 2 that the deposited nanoparticles gather at step-edges and defects, indicating a high mobility of the particles on HOPG and thus only slight substrate–nanoparticle interaction. The nanoclusters can be deposited on a wide range of substrates, such as HOPG, surface-oxidized silicon wafer and glass [17]. It should be noted that on the latter substrates, which exhibit a larger surface roughness, the deposited nanoparticles are not as mobile. Here, the particles lie randomly scattered on the substrate for sub-monolayer depositions [17]. Additionally, thick depositions consisting of multiple layers of individual nanoparticles on top of each other have been demonstrated [12]. For all substrates and thicknesses the microstructure of the deposits is individual nanoparticles, as evidenced by AFM micrographs. These results give strong evidence that the clusters grow in the gas phase. Neither the particle-layer morphology nor the substrate independence of the resulting particles, nor the thick depositions with multiple layers of individual particles, can be explained by any other means, i.e., with surface growth processes.

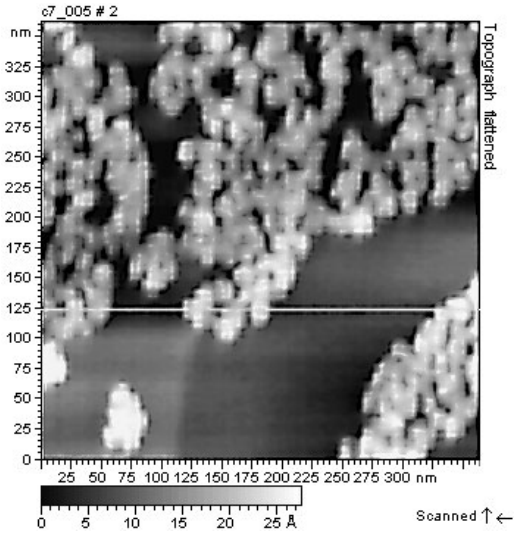

Figure 2. AFM micrograph of nanoparticles on an HOPG surface. The x–y dimensions are 400 nm and the z scale is 2.7 nm. Individual nanoparticles with heights around 2 nm are clearly visible.

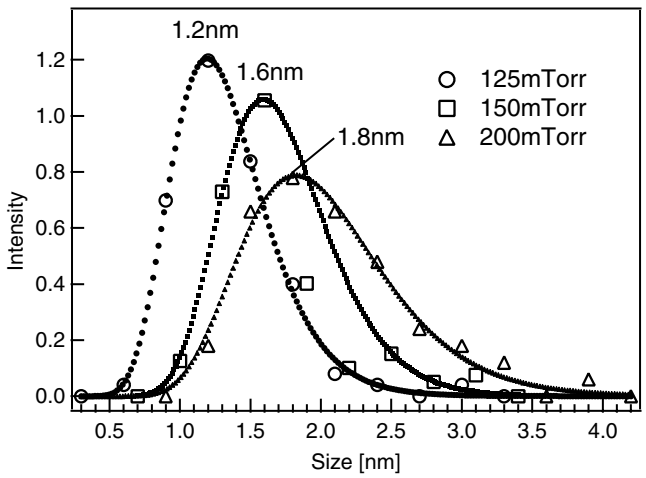

Figure 3. Particle size as a function of argon buffer-gas pressure. The particles have been aggregated with similar evaporation temperatures and the buffer-gas pressure has been altered. The measured particle sizes have been grouped in intervals of 0.3 nm (open symbols) and have been fitted with a log-normal distribution (solid symbols). The peak size of the distributions scales with increasing argon pressure.

3.2. Size analysis

Cluster depositions on HOPG similar to the one shown in figure 2 are performed for determination of the particle sizes with the AFM. HOPG, an almost atomically flat substrate, yields a reliable baseline for the size measurements. In figure 3 particle sizes as a function of argon buffer-gas pressure are shown. All depositions in figure 3 are done with a relative heating current $I_{rel} = 2$ A ($\approx$1100 °C). The buffer-gas pressure is varied from 75 to 300 mTorr, but

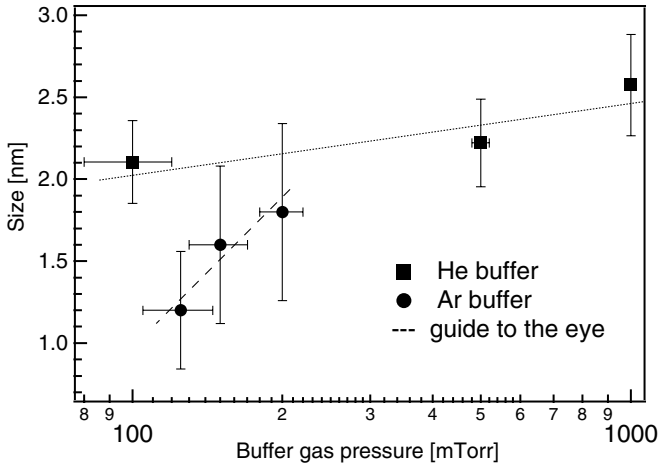

Figure 4. Comparison of sizes as a function of helium and argon buffer-gas pressure, respectively. The particles have been aggregated with similar evaporation temperatures and only the buffer-gas pressure has been altered. While for the argon gas the particle size strongly depends on the pressure, for helium gas the size changes only slightly over a whole order of magnitude of pressure.

only argon pressures between 125 and 200 mTorr yield nanoparticle depositions. Outside the pressure range of 125–200 mTorr no convincing AFM images of individual particles could be obtained. For the size distributions shown in figure 3 particle sizes from multiple AFM micrographs have been counted and grouped in intervals of 0.3 nm (open symbols). The size data in figure 3 are tailed towards larger particles. They can be fitted with a log-normal distribution. For better comparability the area under each curve has been normalized to one arbitrary unit. The absolute FWHM of the distributions increases with increasing particle size. However, it is relatively constant at 60% of the maximum particle size. The peak of the size distribution shifts with increasing argon pressure from 1.2 nm for 125 mTorr argon to 1.8 nm for 200 mTorr argon.

The same study of the particle-size dependence on the buffer-gas pressure is done for helium. The results are summarized in figure 4. For the samples prepared in a helium atmosphere the evaporator is heated to $I_{rel} = 3$ A ($\approx$1150 °C) and the pressure is varied from 100 to 1000 mTorr (note the logarithmic scaling for the buffer-gas pressure on the x axis). In contrast to argon, nanoparticles can be produced in a helium-buffer pressure range covering a whole order of magnitude. However, while argon yields a strong particle size dependence on the pressure in a small range, there is only a small effect in the case of helium. It is noteworthy that this contrasts with the results of metal cluster formation, where for all buffer gases strong size dependences have been observed [18].

The other major parameter for the aggregation process is the partial pressure of the aggregation material, which is proportional to the evaporation temperature and thus to the heating current. In figure 5 the particle sizes as a function of heating current for a helium buffer gas are shown. The helium pressure is set fixed at 500 mTorr and the relative heating current is varied from 1 to 4 A ($\approx$1050–1200 °C). In figure 5 the measured particle sizes are grouped in intervals of 0.2 nm (open symbols) and log-normal functions are fitted to the experimental data (curves). The FWHM of the size distributions is about 25% of the mean size for the depositions with $I_{rel} = 2$ A and above. Only the size distribution with a mean

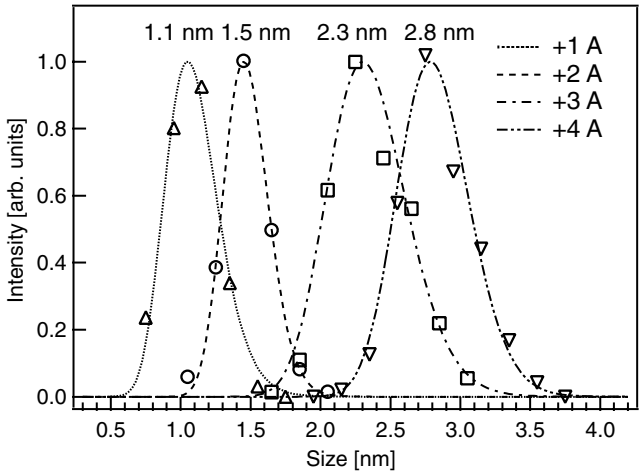

Figure 5. Size distribution as a function of heating current in helium buffer gas with fixed buffer pressure of 500 mTorr. The measured sizes have been grouped in intervals of 0.2 nm (open symbols) and have been fitted with a log-normal distribution (curves). The peak size scales with the evaporation current, i.e., temperature. The current necessary for melting the Ge is $I_{melt} = 13$ A and the numbers in the graph indicate the relative heating current I_{rel} as described in the text. The size distributions are less tailed and narrower than for an argon buffer.

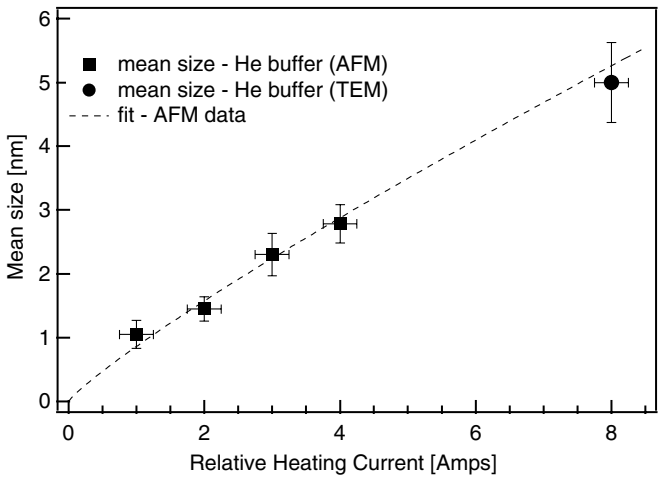

Figure 6. Mean cluster size versus relative heating current in a He buffer-gas atmosphere of 500 mTorr from AFM ($I_{rel} = 1$–4 A) and TEM ($I_{rel} = 8$ A) measurements. The current necessary for melting the Ge is $I_{melt} = 13$ A. The data points for the AFM data correspond to the size distributions from figure 5. Here, the error bars indicate in x the read-out error for the heating current and in y the FWHM of the corresponding size distribution. The error bars for the TEM data-point indicate an assumed size distribution FWHM of 25%. Further details can be found in the text.

particle size of 1.1 nm made at $I = 1$ A is significantly broader and the FWHM is 42% of the mean size. The particle size–heating current dependences for a fixed helium-buffer pressure are summarized in figure 6. In addition to the AFM results discussed in this section

a data point for much larger cluster sizes ($I_{rel} = 8$ A) from the TEM experiments discussed below has been added to the graph. The AFM data can be described with a power-function fit, under the boundary conditions that at the melting point of Ge no particles are generated ($I_{rel} = 0$ A $\Leftrightarrow$ particle size $= 0$ nm). This fit of the AFM data ($I_{rel} = 1$–4 A) also describes the size data from TEM ($I_{rel} = 8$ A) satisfactorily. In this context it is noteworthy that large particles can easily be produced by increasing the evaporation temperature, i.e., heating current. However, similar to the particle size, the deposition rate increases with increasing heating current. For relative heating currents above $I_{rel} = 4$ A more than one monolayer of nanoparticles per second are deposited and thus it becomes difficult to produce sub-monolayer depositions, necessary for exact size measurements with the AFM.

Between the two buffer gases important differences are apparent: for the helium buffer gas (figure 5), the size distributions exhibit a much narrower FWHM, and they are much less tailed towards larger cluster sizes, compared to argon (figure 3). The FWHM of the size distribution for helium, with mean particle sizes of 1.5 nm and above, is only about 25% of the mean particle size, compared to about 60% in case of argon. For argon buffer gas there exists a buffer pressure–size dependence, whereas the resulting sizes are relatively independent from the utilized helium pressure (figure 4). However, for argon it is only possible to generate clusters in a small pressure window from 125 up to 200 mTorr, while in the case of helium particles are formed over a whole order of magnitude of pressure. These differences in the resulting size distributions indicate buffer-gas-dependent variations in the particle growth process.

The cluster aggregation process is generally described with a *nucleation-and-growth* model [14, 18–20]. It has successfully described the generation and size-distribution of metal nanoparticles in static [18] as well as flow-type [20] gas aggregation sources. In the nucleation-and-growth model, the particle growth occurs only in a layer above the evaporator. For metal particles Granqvist and Buhrman have observed that the resulting particle sizes are proportional to the atomic weight and pressure of the buffer gas, which they explained with the stronger confinement of the forming particles to the growth region by heavier gases [18].

The nucleation-and-growth model is also expected to be applicable in principle for germanium nanoparticles. However, there are some important differences between the cluster formation process of metals and semiconductors. It has been reported that germanium is evaporated in Ge_n molecules with $1 \leqslant n \leqslant 7$ at temperatures in the range of 1300 °C [21]. This makes the postulated requirement of a critical particle size for nucleation less stringent, as nuclei for the particle generation are immediately present in the vapour. Also, germanium is a covalently bound material, with a strong geometric structure–size dependence and 'magic numbers' for small clusters [22]. Hunter *et al* [23] have investigated the dissociation energies for size-selected germanium cluster ions. They find that small, i.e. molecular, germanium clusters Ge_n with $n < 10$ have significant larger dissociation energies than larger ones. Upon these results they postulate that germanium clusters with $10 < n < 65$ are aggregations of loosely bound small clusters and that starting at 65 atoms it becomes energetically favourable for the particles to rearrange into bulk spheres [23].

Based on these publications and the gathered experimental results it is believed that the germanium clusters grow by successive capture and coalescence. The atoms and molecules ejected from the evaporator are efficiently cooled by the buffer gas. Their mean free path within the buffer gas is on the order of 10^{-1} mm in the 10^{-1} Torr regime [24]. The existing molecules can immediately serve as nuclei for further growth. The forming particle successively captures and coalesces atoms and molecules out of the supersaturated vapour. The stronger pressure–size dependence for argon as buffer gas can be attributed to the atomic weight of the gases. Argon as the heavier gas confines the forming particles more effectively to the growth region [18].

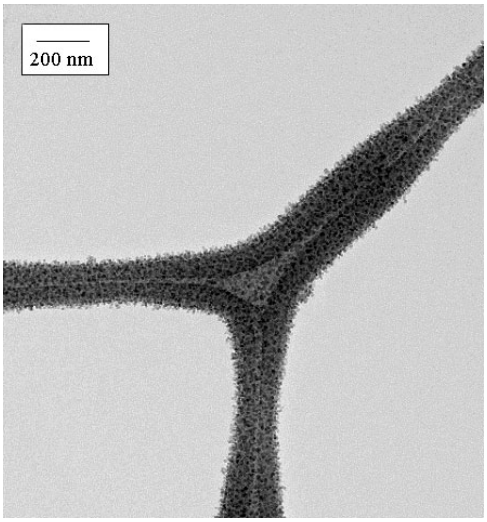

Figure 7. Bright field TEM image of germanium nanoparticles on a lacy carbon grid. The clusters have been directly evaporated onto the grid. A homogenous nanoparticle film is clearly visible.

3.3. Structural analysis

To characterize the geometric structure of the nanoparticles TEM investigations have been performed. The samples for the TEM investigation are prepared by direct evaporation of the clusters on a lacy carbon grid. The synthesis parameters are a relative heating current of $I_{rel} = 8$ A, a helium-buffer pressure of 500 mTorr, and a shutter opening time of 3 s. After the sample preparation a macroscopic amount of particles, visible with the naked eye, is deposited on the sample holder. The nanocrystal samples are transported to the TEM facility in a vacuum suitcase. However, some brief exposure to air and thus oxidation of the nanoparticles could not be avoided.

In figure 7 a conventional bright field image of the nanoparticles is shown. The magnification is about 50 000. In the micrograph the germanium particles appear as dark speckles and a homogenous nanoparticle deposition is apparent. It must be concluded from figure 7 that more than one layer of nanoparticles are deposited on the grid. In figure 8 a high-resolution (HRTEM) micrograph of nanoparticles is shown. The image has been acquired on the edge of a lacy carbon grid string. Sets of randomly orientated lattice planes can be clearly identified. These sets of lattice planes are attributed to individual nanoparticles. It should be mentioned that only particles where the lattice is in adequate orientation to the electron beam exhibit visible lattice planes and can be imaged like that. In this context it should also be emphasized that great care has been taken in the present investigation to avoid crystallization or forced orientation of the particles under the electron beam influence. Figure 8 clearly shows that the particles are crystalline. Additionally it yields further evidence that more than one layer of nanoclusters are deposited and that the particles pile up. One area of overlaid lattice planes is marked with an arrow. An area approximating one particle is surrounded with a dotted circle. On the lower right part of the circle, two sets of lattice planes line up under an angle. This area suggests that two particles exhibit significant surface bond alignment (twinning), indicating strong bonding between these two particles. Twinning cannot be observed for the other particles and thus strong fusion between average particles can be ruled out. The nanocrystals do not exhibit surface facets which have been reported for chemically prepared

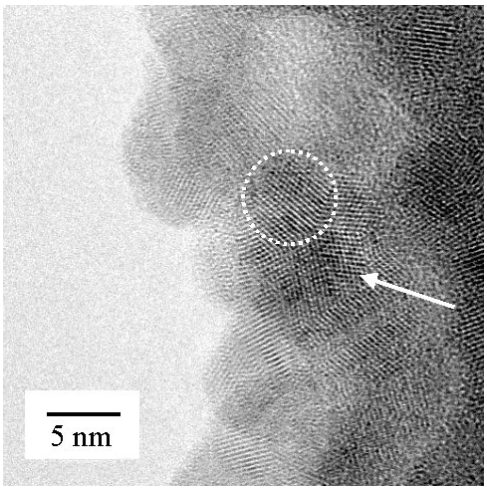

Figure 8. High-resolution transmission electron microscope image of germanium nanoparticles at an edge of a lacy carbon grid. The particles have been directly evaporated onto the grid. The clusters can 'pile up' and an area of overlaid lattice planes is marked with an arrow. The outline of one particle is indicated with a white circle. The particle sizes can be estimated to range around 5 nm.

II–VI nanocluster systems [1]. However, this is expected for the presently investigated gas-phase prepared particles, which have been shown to exhibit a significant amount of surface disorder [12]. Additionally, the surface oxidation due to the brief exposure to air can destroy a potentially ordered surface. The absence of sharp particle boundaries makes exact statements about the particle size and shape impossible. Nevertheless, the particle sizes can be roughly approximated to range around 5 nm. In figure 6 the average size of the TEM sample is compared to the average sizes determined by AFM. The large average particle size of the presently discussed TEM sample ($I_{rel} = 8$ A) is in very good agreement with the dependences between average size and heating current deduced from the AFM investigation for lower heating currents ($I_{rel} = 1$–4 A), indicating similar growth dynamics over a wide range of condensation parameters.

A representative SAD micrograph of the deposited nanoparticles is shown in figure 9. The investigated area is a circular random spot on the sample, with a diameter of a few tens of a nanometre. The diffraction pattern in figure 9 consists of individual diffraction spots on three concentric rings, underlining the polycrystalline character of the probed nanoparticle sample area. The three rings in the diffraction pattern match reference data for the (111), (220) and (311) lattice planes of cubic germanium with reciprocal lattice vectors of 0.31, 0.50 and 0.59 Å^{-1}, and thus it can be concluded that the nanoparticles in the sample are crystalline and exhibit the same diamond crystal structure as the bulk material.

In the literature, there is an ongoing discussion about the crystal structure of germanium nanoparticles. Depending on the preparation method, the bulk-diamond, tetragonal and amorphous phases have been reported. In TEM measurements of 4 nm sized germanium particles embedded in a SiO_2 matrix, Kanemitsu *et al* [25] have observed lattice spacings of 0.298 nm (reciprocal lattice vector of 0.33 Å^{-1}), which they attribute to the (112) plane of the tetragonal germanium phase. Sato *et al* [3] describe x-ray diffraction experiments on germanium particles produced with the cluster-beam evaporation technique. They find a weak diffraction peak for $2\theta = 33°$, which they attribute to the tetragonal germanium (210) lattice plane with a lattice spacing of 0.264 nm (0.38 Å^{-1}), and from their diffraction data they

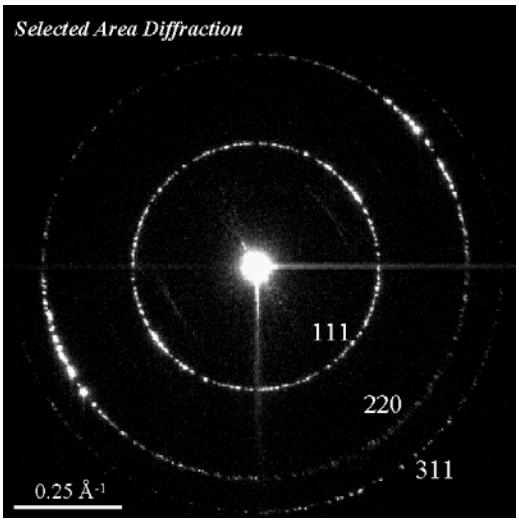

Figure 9. SAD with the transmission electron microscope. In the diffraction pattern individual diffraction spots from various nanocrystals can be clearly identified, underlining the polycrystalline character of the nanocrystal film sample. The azimuthal distance of the diffraction rings corresponds to the diffraction from the Ge 111, 220 and 311 lattice planes.

calculate a mean particle size of 4.3 nm. Jiang *et al* [7] have developed a method for germanium nanocrystal film production by plasma-enhanced chemical vapour deposition. They find by means of x-ray diffraction and TEM analysis amorphous, diamond-like and tetragonal phases of the resulting particle film, depending on the GeH_4/H_2 mixture ratio and substrate temperature. It is interesting to note that Jiang *et al* report only one diffraction peak at $2\theta = 25°$ with a lattice spacing of 0.345 nm (reciprocal lattice vector of 0.29 $Å^{-1}$), which they attribute to the (111) planes of the tetragonal structure, whereas Sato *et al* find only one diffraction peak for $2\theta = 33°$ with a lattice spacing of 0.264 nm (0.33 $Å^{-1}$), which they attribute to the (210) lattice plane of the tetragonal phase. Considering the polycrystallinity of nanoparticle films, the observation of both lattice planes, i.e., diffraction peaks and all other strong lines is expected. In a theoretical study, Pizzagalli *et al* [13] have calculated that germanium nanoparticles are more stable in the diamond phase than in the tetragonal structure, irrespective of particle size for sizes larger than 1 nm. However, they have phenomenologically argued that the energy barrier from the amorphous phase to the tetragonal phase lies lower than the energy barrier between the amorphous and the diamond phase. The present study yields direct evidence for gas-phase aggregated, deposited nanocrystals with sizes around 5 nm to exhibit the cubic phase. This result contradicts the previous experimental studies on similar-sized particles, which have been synthesized with other techniques. For smaller nanoparticle sizes no satisfactorily TEM data could be obtained due to experimental difficulties. Nevertheless, spectroscopic data from x-ray absorption measurements on gas-phase aggregated nanoparticles down to 2.5 nm suggest these particles also exhibit the bulklike, cubic phase [26]. The x-ray absorption spectra of these nanoparticles and bulk germanium are very similar [26]. A phase transition from the cubic to the tetragonal or even amorphous phase in smaller particles is expected to significantly alter the electronic structure of the particles, as reported by Sato *et al* [27] for tetragonal nanoclusters.

The different observed germanium nanoparticle phases can be, at least for the gas aggregation and cluster-beam deposition techniques, understood with the different cluster growth processes. In the cluster-beam evaporation technique of Sato *et al* [3] a beam composed

of atoms and clusters is ejected into a high-vacuum chamber by a supersonic expansion through a nozzle. This process is very fast and the forming particles are rapidly cooled. It is believed that even for larger clusters the aggregation process can be described in the picture of Hunter *et al* [23] as an agglomeration of small clusters. As the agglomerations grow, the developing pressure from the particle surface on the core can induce a phase transition from amorphous to tetragonal particles, in accordance with the predictions of Pizzagalli *et al* [13].

In the gas-aggregation technique of the present study, however, the cluster cooling processes are expected to be significantly slower. The thermal energies of the particles are only transferred by ballistic collisions with the buffer-gas atoms. The cohesive energies in germanium clusters with more than 50 atoms are about 3.2 eV/atom [23], and thus with every added atom a significant amount of energy is deposited in the particle. This allows the atoms in the particle to arrange in the most stable diamond configuration. After they leave the growth zone they are gradually cooled by collisions with the buffer gas, remaining in the diamond phase.

4. Summary

An aggregation source for the generation and non-destructive deposition of germanium nanocrystals has been developed and characterized. Particle size distributions with mean sizes from 1 to 3 nm have been characterized with atomic force microscopy. Larger nanocrystals can be produced but for them the formation and deposition is so efficient that it becomes hard to produce sub-monolayer films of particles suitable for AFM size characterizations. The resulting size distributions depend on the utilized buffer gas, with helium yielding narrower size distributions than argon. HRTEM and SAD have shown that particles with average sizes around 5 nm are crystalline in the diamond phase on both the microscopic level of individual clusters and in a sample-averaging mode. Successive capture and coalescence of atoms and molecules out of the supersaturated Ge vapour has been suggested as the growth mode of the nanocrystals. With this growth mode the resulting buffer-gas-dependent size distributions as well as the formation of individual nanocrystals in the diamond phase can be understood.

Acknowledgments

C Bostedt acknowledges partial financial support from the Deutscher Akademischer Austauschdienst (DAAD) in the HSP-III programme under contract D/97/18881. This work was performed under the auspices of the US Department of Energy by the University of California, Lawrence Livermore National Laboratory under contract no W-7405-Eng-48.

References

[1] Alivisatos A P 1996 *J. Phys. Chem.* **100** 13226
[2] Zacharias M and Fauchet P M 1997 *Appl. Phys. Lett.* **71** 380
[3] Sato S, Nozaki S, Morisaki H and Iwase M 1995 *Appl. Phys. Lett.* **66** 3176
[4] Zhu J G, White C W, Budai J D, Withrow S P and Chen Y 1995 *J. Appl. Phys.* **78** 4386
[5] Ngiam S T, Jensen K F and Kolenbrander K D 1994 *J. Appl. Phys.* **76** 8201
[6] Maeda Y, Tsukamoto N, Yazawa Y, Kanemitsu Y and Masumoto Y 1991 *Appl. Phys. Lett.* **59** 3168
[7] Jiang J, Chen K, Huang X, Li Z and Feng D 1994 *Appl. Phys. Lett.* **65** 1799
[8] Nogami M and Abe Y 1994 *Appl. Phys. Lett.* **65** 2545
[9] Taylor B and Kauzlarich S M 1998 *Chem. Mater.* **10** 22
[10] Wilcoxon J P, Provencio P P and Samara G A 2001 *Phys. Rev.* B **64** 035417
[11] van Buuren T, Dinh L N, Chase L L, Siekhaus W J and Terminello L J 1998 *Phys. Rev. Lett.* **80** 3803

[12] Bostedt C, van Buuren T, Willey T M, Franco N, Möller T and Terminello L J 2002 *J. Electron Spectrosc. Relat. Phenom.* **126** 117
[13] Pizzagalli L, Galli G, Klepeis J E and Gygi F 2001 *Phys. Rev.* B **63** 165324
[14] Haberland H 1994 *Clusters of Atoms and Molecules: Theory, Experiment, and Clusters of Atoms (Springer Series in Chemical Physics vol 52)* (Berlin: Springer)
[15] Kasukabe S 1990 *J. Cryst. Growth* **99** 196
[16] Han W, Lindsay S M and Jing T 1996 *Appl. Phys. Lett.* **69** 4111
[17] Bostedt C 2002 Electronic structure of germanium nanocrystal films probed with synchrotron radiation *PhD Thesis* Universität Hamburg
[18] Granqvist C G and Buhrman R A 1976 *J. Appl. Phys.* **47** 2200
[19] Melinon P, Paillard V, Dupuis V, Perez A, Jensen P, Hoareau A, Perez J P, Tuaillon J, Broyer M, Vialle J L, Pellarin M, Baguenard B and Lerme J 1995 *Int. J. Mod. Phys.* B **9** 339
[20] Panda S and Pratsinis S E 1995 *Nanostruct. Mater.* **5** 755
[21] Kant A and Strauss B H 1966 *J. Chem. Phys.* **45** 822
[22] Martin T P and Schaber H 1985 *J. Chem. Phys.* **83** 855
[23] Hunter J M, Fye J L and Jarrold M F 1994 *Phys. Rev. Lett.* **73** 2063
[24] Brunner W F Jr and Batzer T H 1965 *Practical Vacuum Techniques* (Princeton, NJ: Van Nostrand-Reinhold)
[25] Kanemitsu Y, Uto H and Masumoto Y 1992 *Appl. Phys. Lett.* **61** 2187
[26] Bostedt C, van Buuren T, Franco N, Balooch M, Möller T and Terminello L J 1999 *Electrochem. Soc. Proc.* **99–22** 261
[27] Sato S, Nozaki S and Morisaki H 1998 *Appl. Phys. Lett.* **72** 2460